Transition to space-time chaos in an optical loop with translational transport

L. Pastur, U. Bortolozzo, and P. L. Ramazza
Istituto Nazionale di Ottica Applicata, Largo Enrico Fermi 6, 50125 Firenze, Italy
(Received 30 July 2003; published 28 January 2004)

We describe the transition from regular patterns to space-time chaos in an optical system with nonlocal feedback. The nonlocality introduced breaks the rotational symmetry of the system, resulting in a scenario for the transition from regular patterns to a disordered dynamics. The different regimes are characterized both in terms of spatial and temporal correlation functions, and by means of a Kahrunen-Loeve decomposition. This allows the determination of the structures participating in the dynamics, and an estimation of the active degrees of freedom versus the control parameter.

DOI: 10.1103/PhysRevE.69.016210 PACS number(s): 05.45.Jn, 42.65.Sf, 47.54.+r

I. INTRODUCTION

In the context of the research about disordered dynamical states in extended systems [1], several nonlinear optical systems have recently attracted attention [2–5]. In particular, nonlinear media or devices inserted in optical loops [6,7] offer a powerful framework for the study of pattern formation, both in ordered and in disordered dynamical regimes.

Among such devices, liquid crystal light valves (LCLV's) have become popular because of their large nonlinearity and slow time scale, which allow the study of large aspect ratio, space-time dependent signals.

Indeed, optical valves act over a wide range of optical intensities as Kerr-like media, transforming input intensity distributions $u(\mathbf{r},t)$ into output phase modulations $\varphi(\mathbf{r},t)$ proportional to u. In a diffractive feedback configuration, phase modulations transform by free propagation into amplitude distributions, producing at the rear side of the valve an intensity pattern that will in turn generate phase modulations, hence closing the feedback loop. Such a nonlinear optical system can therefore enhance spatiotemporal perturbations, and lead to pattern formation, beyond some critical value I_c of the input light intensity.

If nonlocal interactions are introduced by means of a translation Δx in the feedback beam, a particularly rich scenario of instabilities is observed; in particular, transitions from hexagons to stripes, and then to bimodal states, nonequilateral hexagons or zig-zag patterns can occur [8]. These situations have been characterized close to threshold; the transition from regular patterns to space-time chaos, on the other side, has been so far studied only in the case $\Delta x=0$ [9–11].

In this paper, we are interested in the scenario of transition toward space-time chaos in an optical loop of this kind for a nonzero value of Δx. The control parameter is the light intensity I at the input of the LCLV, and the spatial offset Δx is set at a value such that stripes are selected at threshold. When the pump parameter is increased, the initially complete order of the structures is first broken by the appearance of local bursts of activity, which can give rise to dislocations. These appears at random positions in the system and determine an anisotropic behavior of the spatial correlation function at intermediate pump values. In this ''weakly chaotic'' situation, the signal displays a limited amount of irregular fluctuations upon an otherwise regular stripe pattern, which contains most of the energy.

The number of active areas and defects increases when increasing the control parameter, and ultimately all signatures of regularity are lost in the signal. In the fully developed chaotic regime, the isotropy of the spatial correlation function is, at least partially, recovered. Furthermore, we will see how the signal manifests a fully multimode nature, contrary to what happens at lower pump values.

In Sec. II we briefly describe our experimental setup, consisting of an optical feedback loop closed trough a LCLV. Section III is devoted to a qualitative description of the route from regular patterns to space-time chaos (STC) observed. In Sec. IV we give a quantitative characterization of the above transition, in terms of spatial and temporal correlation functions. Section V is dedicated to an analysis of the signals in terms of the Kahrunen-Loeve decomposition. This technique allows an identification of the modes participating to the dynamics, and a quantitative evaluation of the number of active degrees of freedom.

II. EXPERIMENTAL FEATURES

The experimental setup is shown in Fig. 1. A liquid crystal light valve is illuminated by an expanded spatially uniform

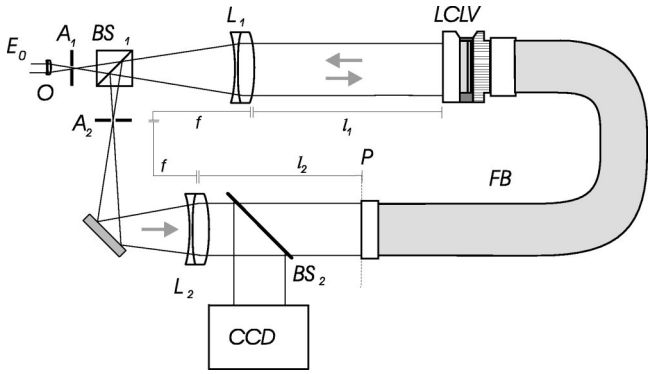

FIG. 1. Experimental setup. An extended laser beam is closed through a nonlinear Kerr-like medium (liquid crystal optical valve). Instabilities develop in the transverse plane of the beam. O: microscope objective; A_1, A_2: apertures; BS_1, BS_2: beam splitters; LCLV: liquid crystal light valve; L_1, L_2: lenses of focal lens f; FB: fiber bundle, twisted of 180° in order to compensate the image spatial inversion introduced by the lenses.

laser beam generated by an Ar^+ laser at 514 nm. The valve operates like a defocusing medium working in reflection. Over a broad range of parameters, a proportionality relation holds between the intensity of the writing light, that reaches the back of the valve, and the phase retardation induced on the reading beam on the front valve face. We will operate within this range, referred to as ''Kerr-like regime,'' in the experiments here reported.

Two lenses L_1 and L_2 realize a one-to-one image of the LCLV front side in a plane that can be placed before or after the input of a fiber bundle. This one relays the image from its input plane P to the back face of the LCLV. The supply voltage applied to the LCLV is $V=8.5$ V, the frequency $\nu=2$ kHz.

The control parameter is the input light intensity $I\equiv|E_0|^2$; in the following, we make use of the reduced control parameter, defined as $\epsilon=I/I_c-1$, where I_c is the threshold intensity for pattern formation.

Beam splitter BS_2 deviates a part of the beam onto a charge-coupled device camera. Time series of $T=200$ snapshots $u(\mathbf{r},t)$ of the beam transverse section in a plane conjugated to P_2 are acquired, and stored as 8-bits 256×256 pixels pictures. The variable x will denote the coordinate in the direction of the translation Δl, y the coordinate perpendicular to it. The sampling time depends on I, decreasing from 200 ms at $I\sim I_c$ to 40 ms in space-time chaos. This dependence follows the natural scale of the dynamics, as will be seen in Sec. IV.

The spatial frequencies at which the system destabilized are those for which the phase distribution is most efficiently converted to intensity distribution, due to the propagation over the effective diffractive length $L=(l_1+l_2)-2f$ ($L=-80$ mm in the experiment here reported). The values of these frequencies are $q_n\simeq\sqrt{k_0\pi(2n+1)/L}$, with n even. How many of these scales are actually excited, will depend on both the input intensity, and the diffusion length of the LCLV. In our case, this length is of the order of 40 μm.

Furthermore, any of these frequencies can generate harmonics, due to the nonlinearity which inherently relates the electric field to its phase. Given, e.g., a phase distribution at a single spatial frequency k_0, and having an amplitude γ, the corresponding electric field is

$$E_0 e^{i\gamma\sin(k_0x)}=E_0\sum_n J_n(\gamma)e^{ink_0x}, \tag{1}$$

which in principle contains all the harmonics of k_0. In practical cases, only the harmonics up to a certain maximum order will contain a relevant amount of energy. The number of these excited frequencies increases for increasing γ.

Due to these mechanisms of frequency destabilization and generation it is possible, in this system to obtain very broadband, ''turbulentlike'' signals.

III. TRANSITION TO SPACE-TIME CHAOS

When the feedback is local, i.e., when no translation is applied to the pattern before feeding it back to the valve ($\Delta x=0$), the selected pattern at the onset I_c of the instability

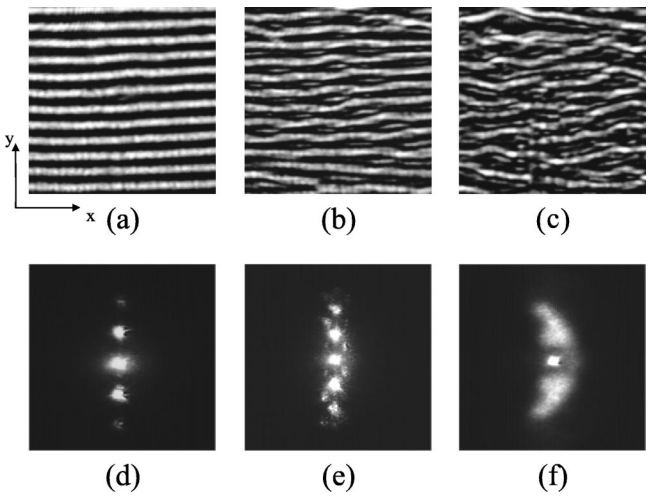

FIG. 2. Patterns observed for increasing ϵ: (a) stripes ($\epsilon=0.6$); (b) varicose state with defects ($\epsilon=3.1$); (c) developed space-time chaos ($\epsilon=6.1$). Upper raw: near field intensity distributions; lower row: Far field intensities.

consists of stationary hexagons. When Δx is increased, hexagons lose stability to the benefit of stripes that are parallel to x. Increasing further Δl up to $\simeq220$ μm, a transition from stripes to a bimodal pattern (horizontal+vertical stripes) occur [8].

We study the transition from regular stripes to space-time chaos keeping fixed $\Delta x=180$ μm, and increasing I. The pattern formation threshold is at $I_c=10$ μW/cm^2. Slightly above this value, a set of stripes of the kind shown in Fig. 2(a) forms. Figure 2(d) represents the far field distribution of Fig. 2(a), corresponding to its Fourier spectrum. It can be seen that the pattern is essentially at a single scale, with a very small amount of second harmonic. This scale, corresponding to the first unstable band q_1, is $\Lambda\simeq285$ μm.

Figure 3(a) displays the time evolution of the central line of Fig. 2(a). Clearly, the pattern is stationary, and hence fully correlated in space and time. At higher pump intensities, the symmetry of these stripes is first broken by the appearance of a varicose mode, at $\epsilon\simeq2$. The features of this instability depend on Δx, and we are not discussing this point in detail here.

The varicose pattern, initially stationary, becomes time dependent at $\epsilon\simeq3$. A snapshot of such kind of structure is

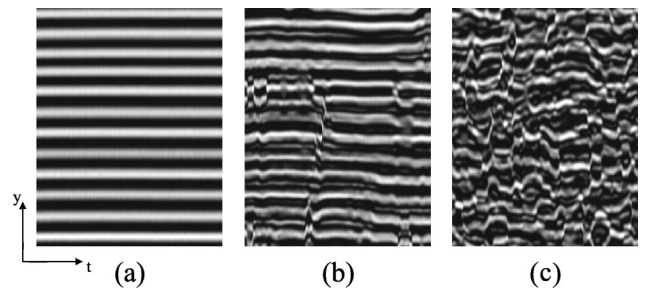

FIG. 3. Space-time diagrams for $\epsilon=0.6$ (a), 3.1 (b), 6.1 (c). The duration of the time series is 20, 12, and 5 sec in (a), (b), and (c), respectively.

shown in Fig. 2(b), and its power spectrum in Fig. 2(e). In these conditions, localized areas in the pattern become temporally active. In some cases the activity is limited to a phase fluctuation that remains localized on a single stripe: in others, defects are created in the form of dislocations, which then propagate in the direction of Δx (towards the right in our figures). The time evolution of a line oriented along y in this regime is visible in Fig. 3(b).

The number of these active areas and their occurrence frequency increases for increasing ϵ, until, at $\epsilon \simeq 5$, a fully space-time chaotic state is reached. In this regime, the instantaneous pattern still displays a visible residual of striped symmetry [Fig. 2(c)]. However, the spectral broadening observed in Fig. 2(f) indicates a loss of spatial correlation over each single frame. The time evolution of a line oriented along y, shown in Fig. 3(c), displays clearly how space-time defects invades now the whole system, leading to a fast time decorrelation at any spatial location.

IV. CORRELATION FUNCTIONS

In order to characterize quantitatively the transition from regular patterns to space-time chaos, we evaluated the spatial and temporal correlation function for several values of ϵ. The spatial correlation function is defined as

$$C_s(\Delta \mathbf{r}) = \left\langle \frac{\langle v(\mathbf{r},t) v(\mathbf{r}+\Delta \mathbf{r},t)\rangle_r}{\langle v(\mathbf{r},t)^2\rangle_r} \right\rangle_t , \tag{2}$$

where

$$v(\mathbf{r},t) = u(\mathbf{r},t) - \langle u(\mathbf{r},t)\rangle_r \tag{3}$$

is the dc filtered pattern. No demodulation is performed on the pattern before computing the correlation functions, since more than one spectral mode develops when increasing ε. The information on the characteristic length along and perpendicular to the stripes will therefore be contained in the envelope of the spatial correlation function.

Sections of $C_s(\Delta \mathbf{r})$ along x and y are shown in Fig. 4 for four increasing values of ε. The correlation decreases along both directions, and more rapidly for higher values of pump than for lower ones. This is of course to be expected.

The other information conveyed by Fig. 4 is that the spatial correlation does not always decay symmetrically along x and y. This symmetry approximately exists close to the pattern formation threshold, and, partially, in the fully developed space-time chaos regime. In the first case, actually, it is expected that, in the absence of experimental imperfections, the correlation length be infinite along any direction. At intermediate values of ε, corresponding to the partially developed chaos, the signal systematically decorrelates faster along y than along x. This behavior is particularly visible at long range ($\Delta r \gtrsim 0.5$ mm) in Figs. 4(b) and 4(c). Here, the correlation function along x is higher than that along y by 30–50%.

The qualitative origin of this asymmetry can be understood by inspection of Fig. 2(b). Here we see that the varicose undulations occurring on different stripes are mutually dephased in an irregular way. Also, at these pump values the undulations are not extended uniformly over the system size along x, but rather appear from time to time in some preferred regions. In these areas, some extra segment of stripes can appear. These structures are clearly visible in Fig. 2(b), and are responsible for the power contained in the second harmonic peaks in Fig. 2(e). These features lead to a rather strong symmetry breaking of the pattern along y. Along x, on the other side, the dominant aspect of the structure is a long wavelength modulation, which affects the correlation loss to a lesser extent.

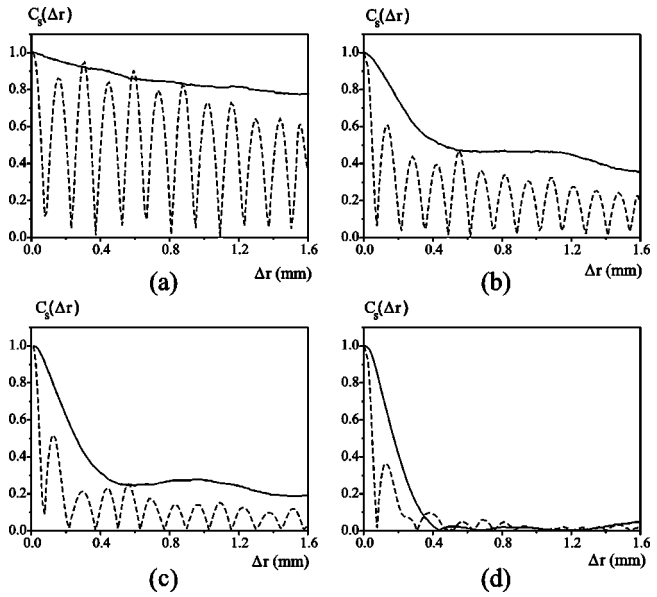

FIG. 4. Spatial correlation functions along x (solid lines) and y (dashed lines). $\epsilon = 0.6$ (a), 3.1 (b), 5.0 (c), 6.1 (d).

The symmetry of the correlation function is partially recovered in the fully developed space-time chaotic regime [Fig. 4(d)], due to the fact that now the stripes appear broken and their residuals are randomly bent with respect to the x axis. However, at short scales ($\Delta r \lesssim 0.3$ mm) the correlation decreases faster along x than along y also in this case.

We then evaluated the global time correlation of the signal. This represents the time coherence of the whole pattern with respect to itself, and is defined as

$$C_t(\Delta t) = \left\langle \frac{\langle v(\mathbf{r},t) v(\mathbf{r},t+\Delta t)\rangle_r}{(\langle v(\mathbf{r},t)^2\rangle_r \langle v(\mathbf{r},t+\Delta t)^2\rangle_r)^{1/2}} \right\rangle_t . \tag{4}$$

This quantity is plot for several values of ε in Fig. 5. The time scale over which the pattern loses correlation varies from tens of seconds, close to threshold, to a fraction of a second in the STC regime. Interestingly, at intermediate values of ε (3.1,4.0) the time correlation does not decay to zero even at long times.

The reason for this can be understood with reference to Fig. 6, showing the time averaged patterns in the regular, partially developed and fully developed STC regimes. The relevant fact here is that, in the partially developed chaos [Fig. 6(b), $\varepsilon = 3.1$], the average structure is still strongly regular. The presence of regularities in the average signal

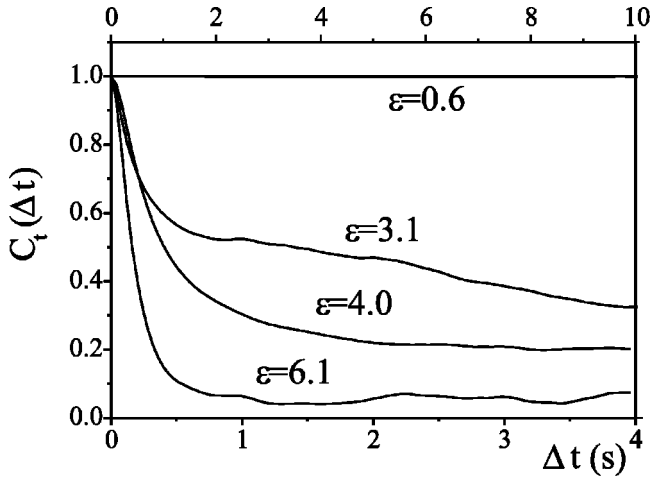

FIG. 5. Time correlation function at several values of ε. The curves at $\varepsilon = 0.6$ and 3.1 are to be referred to the top time axis. The curves at $\varepsilon = 4.0$ and 6.1 are to be referred to the lower time axis.

resulting from space-time chaotic data series has been already pointed out in fluid experiments [12,13].

This symmetry in the averages means that the spatial fluctuations $v(\mathbf{r},t)$ have a very strong time correlated component, which manifests in the finite plateau of the correlation functions shown in Fig. 5. The situation is different in the well-developed STC regime; here the time averaged pattern is the one shown in Fig. 6(c), i.e., gray with only some fluctuations. These ones are probably due to imperfections in the LCLV homogeneity, and are responsible for the small, though nonzero value of the time correlation at $t \to \infty$ observed also in this case.

V. THE KAHRUNEN-LOEVE DECOMPOSITION

In this section, we apply the Kahrunen-Loeve (KL) technique for characterizing the space-time chaotic regime. The KL decomposition is a long used technique in signal analysis and processing [14]. While other techniques of decomposition deal with fixed basis functions [e.g., cos() and sin() for the Fourier transform], the KL technique is aimed to extract from a pattern series the empirical eigenpictures that best fit the statistical set features. Furthermore, it is possible to order these eigenpictures with respect to their ''energy,'' meant as their contribution to the image series dynamics. Doing so, it is often possible to identify a small set of modes which contains most of the relevant information.

This technique has been used in nonlinear dynamics with

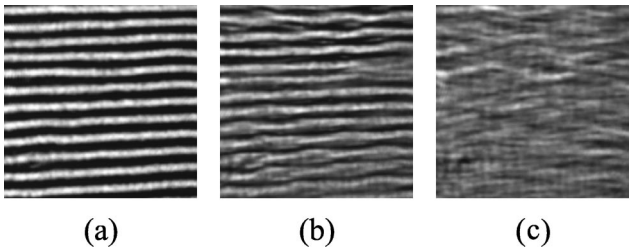

FIG. 6. Time-averaged patterns for $\epsilon = 0.6$ (a), 3.1 (b), 6.1 (c).

the aim of getting out relevant information from turbulent fields [15]. Its success encouraged to extend the method to other physical situations, among which is the study of space-time chaos [16–23].

The data used in this section are, for each value of ε, a set of $T=120$ frames, of $N=512\times512$ pixels per frame. We rearrange these data in a matrix $A(z_m,t_k)$ such as its columns are the $v(x_i,y_j,t_k)$ $[m\equiv(N-1)\dot{i}+j]$ patterns, ranked in a time-increasing order. The matrix A is therefore of size $N\times T$.

Let us briefly recall how the Karhunen-Loève technique works. Given a time series of images $v(\mathbf{r},t)$, the aim is to find two sets of orthonormal functions $\phi_n(t)$, $\psi_n(\mathbf{r})$ such that

$$v(\mathbf{r},t)=\sum_{n\geqslant 1}\mu_n\phi_n(t)\psi_n(\mathbf{r}), \tag{5}$$

where the functions $\{\psi_n(\mathbf{r})\}$ describe the data information content in the spatial domain, and are therefore sometimes called the ''topos.'' Analogously, the $\{\phi_n(t)\}$ are named the ''chronos.'' The set of functions $\psi_n(t)$ are the solutions of the eigenvalue problem having as a kernel the space correlation matrix:

$$K(z_i,z_j)=A^T\cdot A, \tag{6}$$

where T represents the transposition operator. The $\{\phi_n\}$ are further determined by projecting each data picture on the $\{\psi_n\}$ and averaging on space:

$$\phi_n(t)=\frac{1}{\mu_n}\langle v(\mathbf{r},t)\cdot\psi_n(\mathbf{r})\rangle_{\mathbf{r}}. \tag{7}$$

The expansion coefficients μ_n in Eq. (5) are given by

$$|\mu_n|^2=\lambda_n, \tag{8}$$

$\{\lambda_n\}$ being the eigenvalues associated to $\{\phi_n,\psi_n\}$. Since the $\{\psi_n\}$ and $\{\phi_n\}$ are normalized, this amounts to say that the eigenvalue associated to each function represents its ''energy contribution'' to the data series.

Having obtained the KL spectrum, an approximated reconstruction of the pattern is obtained by truncating the expansion (5) up to the n_0th mode (Galerkin projection):

$$v(\mathbf{r},t)\simeq v_{n_0}(\mathbf{r},t)=\sum_{n=1}^{n_0}\mu_n\phi_n(t)\psi_n(\mathbf{r}), \tag{9}$$

where $n_0\leqslant T$.

Typical eigenvalues spectra (usually called *singular spectra*) are reported in Fig. 7 for several values of the pump parameter ε. For small ε, most of the energy is contained in the first eigenpicture [Fig. 8(a)]. As ε is increased, the spectrum tail level grows, while the energy of the first mode decreases: the spectrum becomes flatter and flatter, indicating a tendency towards equipartition of energy among all modes in the developed STC regime.

Figure 8 shows examples of the spatial eigenmodes $\psi_n(\mathbf{r})$, evaluated close to threshold and in the space-time

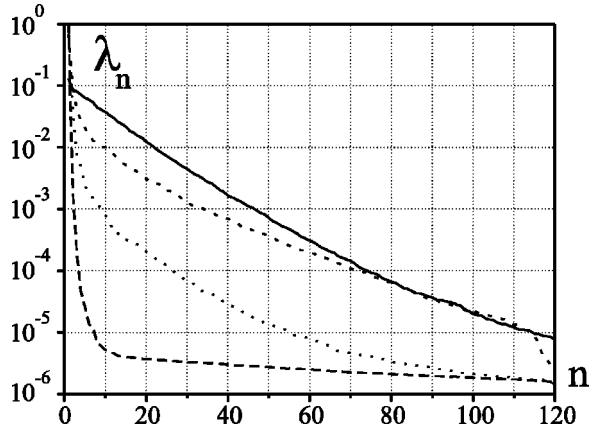

FIG. 7. Singular spectra. $\epsilon = 0.6$ (long dash), 2.3 (dot), 3.1 (short dash), 6.1 (solid).

chaotic regime. In agreement with Fig. 7, one can see that the high order modes [$n = 15$ in Fig. 8(c)] have a relevant amount of information in the case of STC signals, while they represent just a small noise in the regular regime.

We report on Fig. 9(a) how the fraction of energy W_1 contained in the first eigenmode varies vs ε. W_1 is defined as

$$W_1 \equiv \frac{\lambda_1}{\sum_{n=1}^{T} \lambda_n}. \tag{10}$$

This quantity exhibits a smooth transition in the region $2 \lesssim \varepsilon \lesssim 6$, passing from almost 100% to about 10%.

Complementary, Fig. 9(b) shows the number n_0 of modes needed to contain 75% of the total energy of the time series, as a function of ε. Again, a large increase of n_0 can be located at the smooth transition to STC.

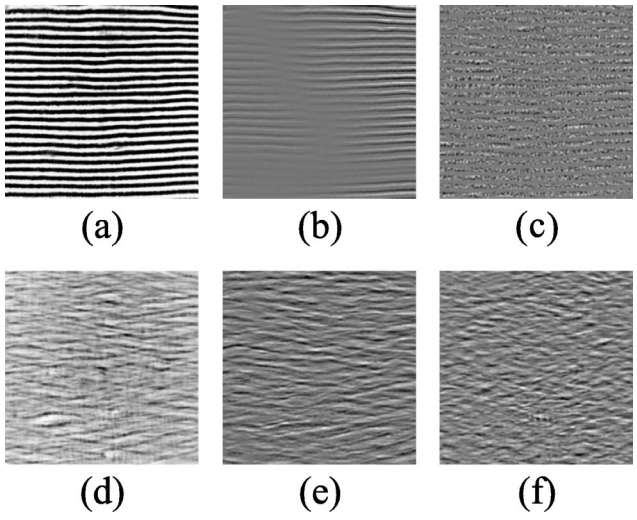

FIG. 8. Some eigenpatterns of the POD: (a,d) first mode, (b,e) second mode, (c,f) 15th mode. Upper raw: $\epsilon = 0.6$, lower raw: $\epsilon = 6.1$.

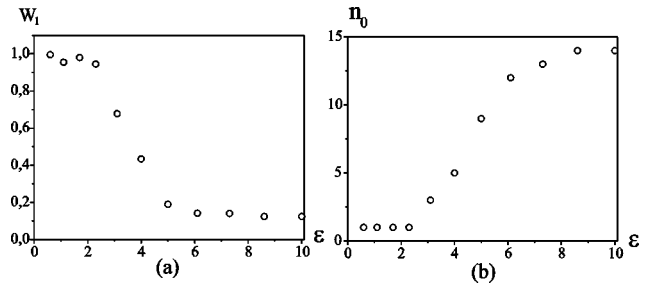

FIG. 9. (a) Energy W_1 contained in the first eigenpattern. (b) Number n_0 of modes required for recovering 75% of the total energy W_T.

Let us introduce the cross-correlation indicator $C(n_0)$ to quantify the quality of the reconstruction between the input pattern v and the pattern v_{n_0} reconstructed using n_0 eigenpatterns:

$$C(n_0) = \left\langle \frac{\langle v_{n_0}(\mathbf{r},t) v(\mathbf{r},t) \rangle_r}{\langle |v(\mathbf{r},t)|^2 \rangle_r^{1/2} \langle |v_{n_0}(\mathbf{r},t)|^2 \rangle_r^{1/2}} \right\rangle_t . \tag{11}$$

This quantity is plotted as a function of n_0 in Fig. 10 for three values of ε. Even in the chaotic regime, a number of modes $\lesssim 20$ appears sufficient to reconstruct a space-time series having a correlation larger than 90% with the original data set.

VI. CONCLUSION

We have presented a scenario of transition from regular patterns to space-time chaotic dynamics, occurring in the presence of a translational transport introduced in an optical system. The main aspects of the route to disorder are the presence of a varicose instability of the initial stripe pattern; the appearance of localized bursts of activity as the first elements destabilizing the ordered structures; the presence of

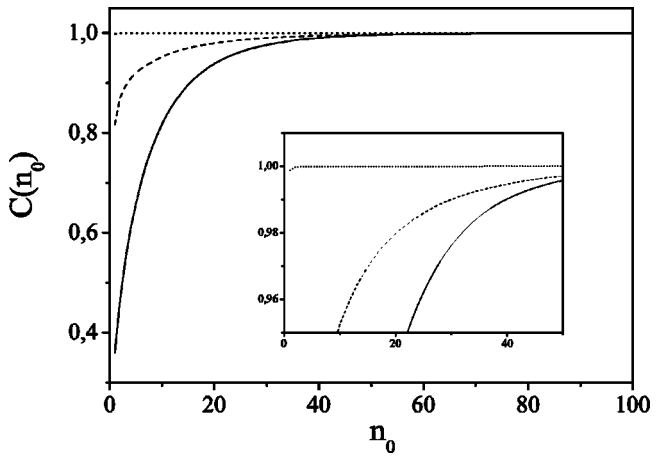

FIG. 10. Cross-correlation indicator $C(n_0)$ quantifying the level of correlation between the pattern and its reconstruction using the first n_0 eigenpatterns for $\epsilon = 0.6$ (dotted line), $\epsilon = 3.1$ (deshed line), $\epsilon = 6.1$ (solid line).

an asymmetry in the spatial correlation function at intermediate values of the pump parameter, and the partial recovery of the symmetry in the fully developed space-time chaos regime.

An analysis of the signals based on the Kahrunen-Loeve decomposition shows that the transition to chaos is very smooth, involving the successive activation of more and more spatial modes over a wide range of the control parameter.

ACKNOWLEDGMENTS

This work was partly supported by EU Contract No. HPRN-CT-2000-00158 and MIUR-FIRB Project No. RBNE01CW3M-001.

[1] See, for example, *Space-Time Chaos: Characterization, Control and Syncronization*, edited by S. Boccaletti, H.L. Mancini, W. Gonzalez-Viñas, J. Burguete, and D.L. Valladares (World Scientific, Singapore, 2001).
[2] J.V. Moloney, P. Jakobsen, J. Lega, S.G. Wenden, and A.C. Newell, Physica D **68**, 127 (1993).
[3] M.A. Vorontsov, J.C. Ricklin, and G.W. Carhart, Opt. Eng. **34**, 3229 (1995).
[4] F.T. Arecchi, S. Boccaletti, and P.L. Ramazza, Phys. Rep. **318**, 1 (1999).
[5] F. Encinas-Sanz, I. Leyva, and J.M. Guerra, Phys. Rev. Lett. **84**, 883 (2000).
[6] S.A. Akhmanov, M.A. Vorontsov, and V.Y. Ivanov, JETP Lett. **47**, 707 (1988).
[7] G.P. D'Alessandro and W.J. Firth, Phys. Rev. Lett. **66**, 2597 (1991).
[8] P.L. Ramazza, S. Boccaletti, and F.T. Arecchi, Opt. Commun. **136**, 267 (1997).
[9] G. D'Alessandro and W.J. Firth, Phys. Rev. A **46**, 537 (1992).
[10] F. Castaldo, D. Paparo, and E. Santamato, Opt. Commun. **143**, 57 (1997).
[11] G. Schliecker and R. Neubecker, Phys. Rev. E **61**, R997 (2000) and references therein.
[12] B.J. Gluckman, P. Marcq, J. Bridger, and J.P. Gollub, Phys. Rev. Lett. **71**, 2034 (1993).
[13] L. Ning, Y. Hu, R.E. Ecke, and G. Ahlers, Phys. Rev. Lett. **71**, 2216 (1993).
[14] See, for example, R.C. Gonzales and P. Wintz, *Digital Image Processing* (Addison-Wesley, New York, 1977).
[15] N. Aubry, P. Holmes, J.L. Lumley, and E. Stone, Physica D **37**, 1 (1989).
[16] L. Sirovich and J.D. Rodriguez, Phys. Lett. A **120**, 211 (1987).
[17] A.M. Fraser, Physica D **34**, 391 (1989).
[18] L. Sirovich, Physica D **37**, 126 (1989).
[19] R. Vautard and M. Ghil, Physica D **35**, 395 (1989).
[20] S. Ciliberto and B. Nicolaenko, Europhys. Lett. **14**, 303 (1991).
[21] S.M. Zoldi, J. Liu, K.M.S. Bajaj, H.S. Greenside, and G. Ahlers, Phys. Rev. E **58**, R6903 (1998).
[22] S.M. Zoldi and H.S. Greenside, Phys. Rev. Lett. **78**, 1687 (1997).
[23] M.P. Chauve and P. Le Gal, Physica D **58**, 407 (1992).